FREQUENCY RATIO ASSESSMENT FOR LANDSLIDES TRIGGERED BY 6 FEBRUARY 2023 KAHRAMANMARAS TURKIYE EARTHQUAKES BETWEEN GOLBASI AND ERKENEK

S. Cetinkaya[1,2], N. Tunar Ozcan [3], G. Karakas [1,2], V. E. Karakas[4], S. Kocaman[2]*, C. Gokceoglu [3]

[1] Hacettepe University, Graduate School of Science and Engineering, Ankara, Türkiye – sinemcetinkaya@hacettepe.edu.tr, gizem.karakas@hacettepe.edu.tr
[2] Dept. of Geomatics Engineering, Hacettepe University, 06800 Beytepe Ankara, Türkiye - sultankocaman@hacettepe.edu.tr
[3] Dept. of Geological Engineering, Hacettepe University, 06800 Beytepe Ankara, Türkiye - ntunar@hacettepe.edu.tr, cgokce@hacettepe.edu.tr
[4] General Directorate of Mineral Research and Exploration, Sogutozu, Ankara, Türkiye - veyselemre.karakas@mta.gov.tr

KEY WORDS: Landslides, Frequency Ratio, 6 February 2023 Kahramanmaras Türkiye Earthquakes, Spatial Statistics, Aerial Photogrammetry

ABSTRACT:

Landslides triggered by earthquakes are significant geological hazards that can have devastating consequences, posing risks to human lives, infrastructure, and the environment. These seismic events may cause the instability of slopes and result in the displacement of soil and rock materials, leading to landslides. It is crucial to understand the characteristics and mechanisms of earthquake-triggered landslides in order to effectively manage and mitigate their associated risks. The number of landslides triggered by the 2023 Kahramanmaraş earthquakes (with magnitudes of 7.7 and 7.6) was over three thousand and their destructive effects were also devastating as secondary hazards. This study aims to examine the characteristics of landslides using the frequency ratio (FR) model. A landslide susceptibility map (LSM) was also produced using the output. For this purpose, in this study, we derived landslides triggered by the earthquakes in a part of the earthquake-affected region, between Golbasi town of Adiyaman and Erkenek village of Malatya covering an area with a size of 625 km^2. The study utilized a landslide inventory that was manually delineated by visual interpretation based on pre-event and post-event. These associations can serve as a foundation for the application of various data-driven machine learning techniques. The findings of this study will contribute to the development of accurate LSMs, providing crucial insights into the behavior of earthquake-triggered landslides.

1. INTRODUCTION

Landslides are among the most destructive nature-triggered hazards, that endanger human lives and infrastructures all over the world. The occurrence and expansion of landslides are influenced by various factors, which can be broadly categorized as conditioning and triggering factors. Conditioning factors include geological factors such as lithology, terrain properties, and topography and the other factors such as vegetation cover, land-use changes depending on the geographical characteristics. The triggering factors refer to the external forces that can initiate a landslide event, such as intense rainfall, earthquakes, volcanic eruptions, and human-induced vibrations. The interaction and interdependence of these factors contribute to the complexity of landslide occurrence, making it essential to consider multiple variables when assessing landslide hazards and risks.

Landslide susceptibility can be defined as a measure of the likelihood or probability of a landslide occurring in a particular location, given the characteristics of the terrain and the environmental conditions. Landslide susceptibility mapping (LSM) is the first step of evaluating the disaster risks. The production of high-quality hazard models requires complete and accurate landslide inventories. The Frequency Ratio (FR) model is widely utilized for assessing the correlations between spatial data and criteria by determining the likelihood of occurrence and non-occurrence for each category of conditioning factors (Dao et al., 2020; Karakas et al., 2021; Pham et al., 2021). This analysis helps to identify the most significant factors contributing to the occurrence of the phenomenon and informs decisions related to risk management and mitigation strategies. Furthermore, FR has been utilized by researchers in conjunction with various approaches to generate landslide susceptibility maps (Khan et al. 2019; Sonker et al., 2022).

The aim of this study is to analyze the characteristics of the landslides using the FR model for the purpose of producing accurate LSMs. The landslides triggered by the 2023 Kahramanmaraş earthquake (Mw 7.7 and 7.6) were taken as a case. In this case, the inventory based on the event was manually delineated by visual interpretation of pre- and post-event aerial photogrammetric images. The FR method was employed with 9 conditioning features to establish the associations between the effective factors and landslide distributions, which can form the basis for the application of diverse data-driven machine learning methods. On the other hand, the calculated FR value of the features was used to generate the LSM.

2. MATERIALS AND METHODS

Earthquakes are among the major factors triggering landslides in areas prone to both hazards. The recent Kahramanmaras earthquakes (Mw 7.7 and Mw 7.6) occurred on 6 February 2023 affected an enormous area with 11 provinces of Türkiye and size

* Corresponding author

of over 100000 km^2. The number of landslides triggered by the event was exhaustive and they yielded destructive effects. Here, in order to understand the main characteristics of the co-seismic landslides, we have quantitatively evaluated the inventory and a number of features that are frequently considered as conditioning factors in the literature using the FR method for one region. A LSM was also produced from the FR values. The overall methodological workflow for LSM of the study area is presented in the Figure 1.

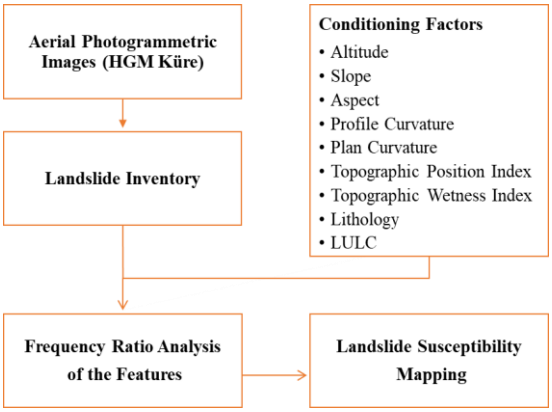

Figure 1. Methodological workflow of the study.

2.1 Study Area and Landslide Inventory

The study area is located between Golbasi (Adıyaman) and Erkenek (Malatya), covers an area of approximately 625 km^2 (Figure 2). A number of research groups including ours initiated immediate assessment of the landslides by establishing actual inventories mainly based on aerial photogrammetry and satellite images. Although remotely piloted aircraft systems (RPAS) were also utilized in some areas, the enormity of the region affected by the earthquakes has indicated that the aerial photogrammetric datasets obtained from an airplane by the General Directorate of Mapping (GDM, 2023), Türkiye were the optimal data sources for rapid inventory compilation and evaluation. Based on the pre- and post-event aerial photogrammetric images of the GDM (HGM Küre), we mapped 323 landslides in the study area.

The study area is located near the triple junction region between the African, Arabian, and Anatolian plates. The Dead Sea Fault Zone (DSFZ) separates the Arabian and African plates, while the East Anatolian Fault Zone (EAFZ) is a complex plate boundary structure between the African and Anatolian plates. The present tectonic structure of the region is shaped by the DSFZ, the EAFZ, and associated intracontinental structures (Reilinger et al., 2006). The study area extends from the southern end of the Celikhan - Erkenek segment of the EAF zone and continues along the Golbasi - Turkoglu segment. The Celikhan - Erkenek segment is characterized as a left-lateral strike-slip fault with an approximate length of 45 km and strikes N67E (Şaroğlu et al., 1992). The Golbasi - Turkoglu Segment is 90 km long and has a strike of K55D. After the Kahramanmaras earthquake series, the largest measured displacement in this segment is more than 6.5 m (AFAD, 2023).

The lithological units within the study area, aging from the Ordovician to the Quaternary, outcrop. The stratigraphy in the northern and southern parts of the area is different from each other due to tectonic contact. The main lithological units in the study area are basic and ultrabasic rocks from the ophiolitic series, clastic rocks, carbonaceous rocks, neritic limestones, and Quaternary alluvium deposits (Çıplak, 2004).

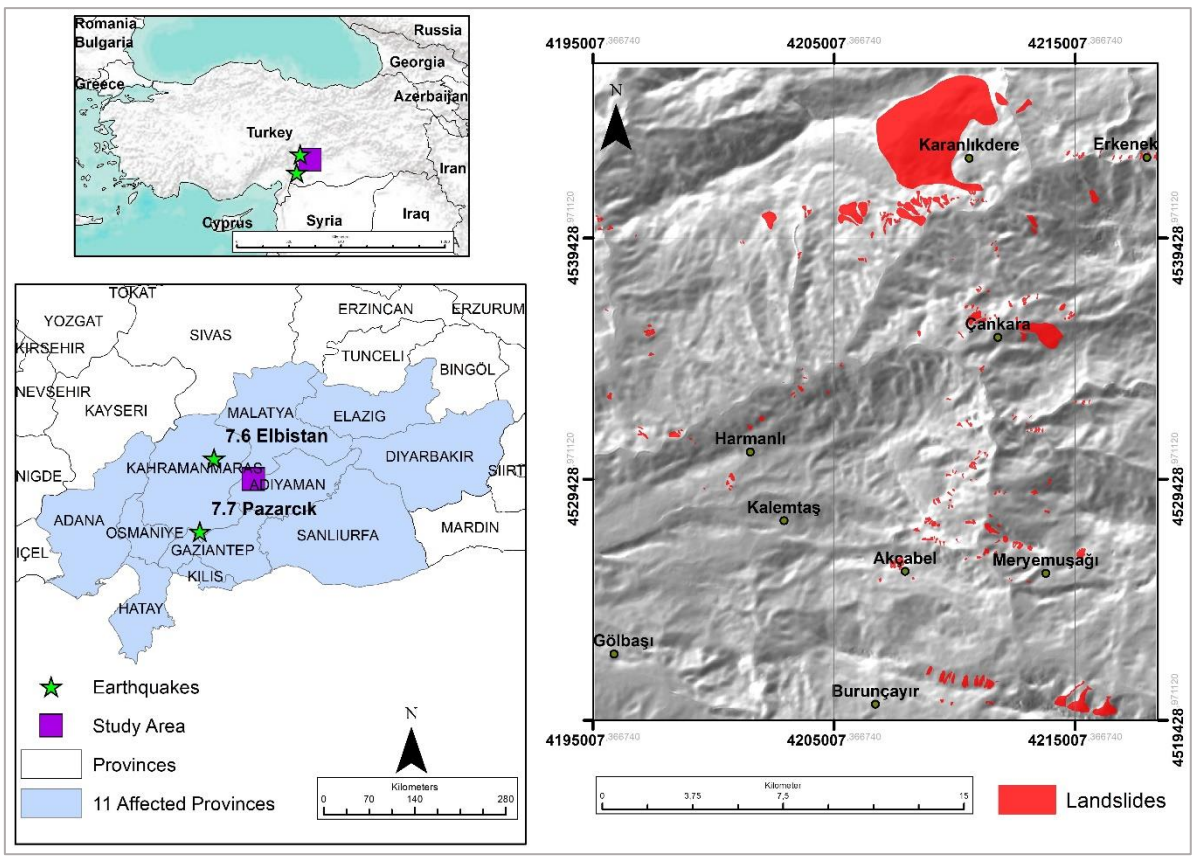

Figure 2. The location map of the study site and the landslide inventory presented on the EU-DEM v1.1.

2.2 Conditioning Factors

As the aerial photogrammetric digital elevation model (DEM) of the area was not yet provided, EU-DEM v1.1 (EEA) was used to generate the conditioning factors: altitude, slope, topographic wetness index, aspect, profile and plan curvature. The efficiency of using EU-DEM v1.1 was proven in previous landslide susceptibility assessment studies (e.g., Karakas et al., 2022). The land use land cover (LULC) obtained from ESA WorldCover (Zanaga, 2022), lithology and faults obtained from the General Directorate of Mineral Research and Exploration (MTA) (Akbas et al. 2016) were also considered as input factors. A total of 1.013.390 pixels (9 features with 11.408 landslides and 1.001.982 non-landslide pixels in each with 25 m grid spacing) were analyzed to reveal the characteristics of the landslides (Figure 2). A total of 9 features were categorized depending on the literature to assess the FR (Karakas, 2021).

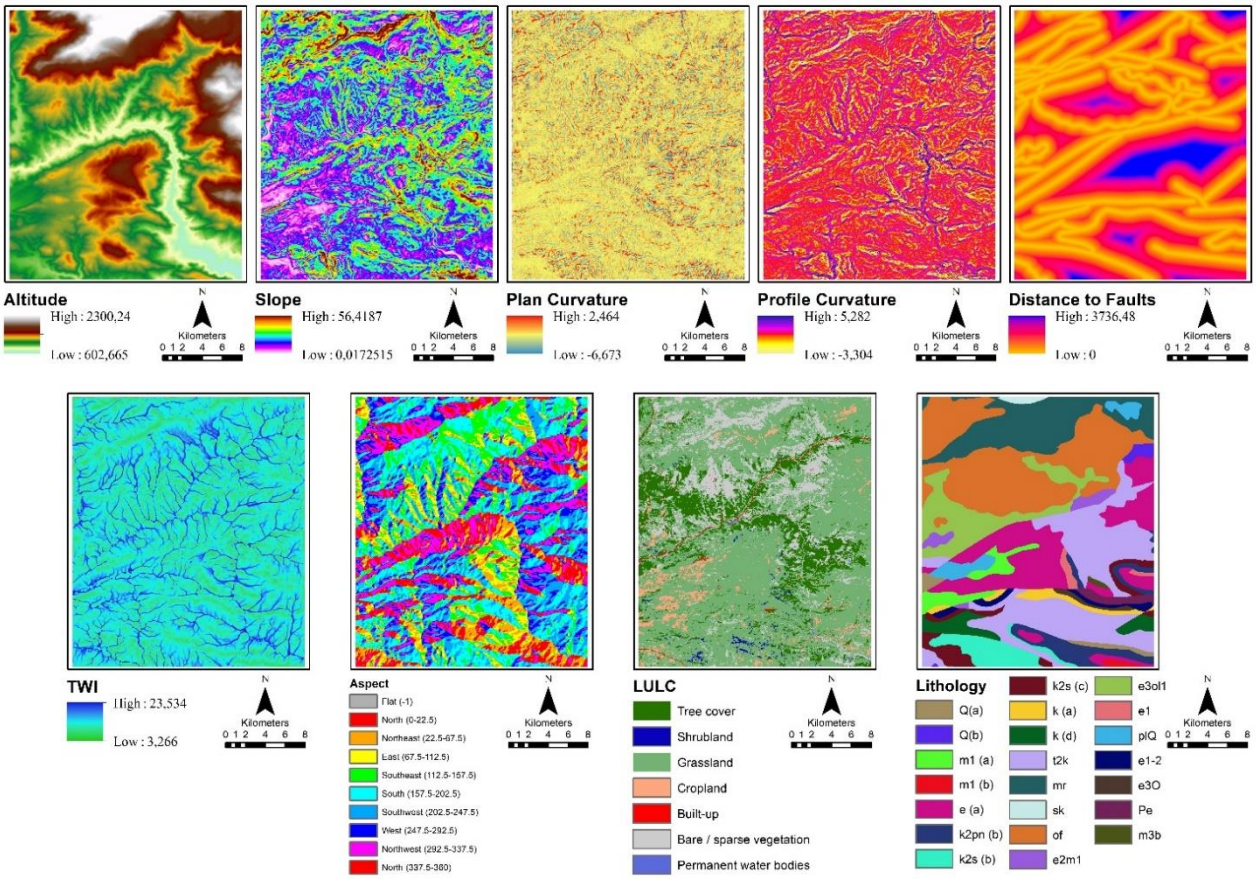

Figure 3. Conditioning factors of the study area: altitude, slope, plan curvature, profile curvature, distance to faults, topographic wetness index (TWI), aspect, lithology, LULC.

2.3 Frequency Ratio Analysis of the Conditioning Factors

The Frequency Ratio (FR) method is one of the commonly utilized statistical analysis techniques in the generation of landslide susceptibility maps (Nefeslioglu et al., 2012; Karakas et al., 2022). The FR has proven to be an effective tool for assessing landslide susceptibility by considering the spatial relationship between landslide events and various conditioning factors.

The main objective of this method is to determine the density of input features that contribute to landslide events. This density is computed by overlaying landslide inventories with feature maps. By analyzing the number of pixels associated with landslide occurrences for each parameter, the FR values are calculated by dividing the percentage of landslide occurrences within the feature by the areal proportion of the feature across the entire study site. Equation 1 provides the formula for calculating the FR.

$$FR = \frac{N_{Li} / N_{Lt}}{N_{Ci} / N_{Ct}} \qquad (1)$$

where N_{Li}i: number of pixels with landslide in feature *i*
N_{Lt}: total number of pixels in landslide inventory
N_{Ci}: total number of pixels in feature *i*
N_{Ct}: total number of pixels in study area

In quantitative analysis, if the computed value of the FR pertaining to the association between landslide occurrences and their condioning factors exceeds 1, it indicates a stronger relationship. Conversely, if the computed FR value falls below 1, it suggests a weaker relationship between the variables (Sonker et al., 2022).

2.4 Landslide Susceptibility

In this section, each evaluated FR value of the features normalize as NFR, and LS is computed based on Equation 2.

$$LS = \sum NFR_n \qquad (2)$$

where, NFR_n the normalization values of FR for each feature per pixel.

3. RESULTS AND DISCUSSIONS

The FR results of the study area were calculated based on Equation 1 for each conditioning factors and provided in Tables A1, A2 and A3 (in Appendix). Altitude plays a crucial role in landslide occurrences, as evidenced by the FR results. Higher altitudes, specifically within the range of 1357.14 - 1545.76 meters and 1545.76 - 1734.38 meters, exhibit a significantly higher FR of 3.13 and 3.02, respectively. This indicates a pronounced correlation between higher altitudes and increased likelihood of the landslides triggered by the Kahramanmaraş earthquakes. The degree of slopes significantly influences landslide occurrences, as indicated by the FR analysis. Steeper slopes, particularly those within the range of 37° - 44° and 44° - 60° degrees, exhibited high FRs of 10.1 and 14.33, respectively. The aspect of a slope, defined by its orientation, also affects landslide occurrences. The FR results indicate that southeast-facing slopes (SE) demonstrate a substantially higher FR of 3.18, suggesting a strong correlation between this aspect and landslides. Plan and profile curvature influence landslide occurrences, as the FR analysis highlights. Negative values of plan and profile curvature, particularly within the range of -1.01 to -1, demonstrate a significantly higher FR, indicating a higher probability of landslides. The topographic wetness index (TWI), which reflects the moisture content of a landscape, is a crucial factor in landslide occurrences. The FR analysis reveals those areas with moderate TWI values, specifically within the range of 10.02 - 12.27 and 12.27 - 14.53, displayed higher FRs of 1.69 and 1.13, respectively.

The proximity to faults affected landslide occurrences, as indicated by the FR results. The analysis demonstrated that smaller distances to faults, specifically within the range of 0-416.08 meters, showed a higher FR of 1.23, suggesting a strong correlation. In Table A3, certain lithological types exhibit higher FR values, indicating an elevated susceptibility to landslides. For instance, neritic limestone and marble/schist exhibit high FRs of 3.95 and 5.75, respectively. Land use and land cover have a profound influence on landslide occurrences, as evidenced by the FR analysis. The results demonstrate that areas with bare/sparse vegetation and grassland exhibit higher FRs of 1.69 and 1, respectively.

To produce the LSM based on the FR method, the *LS* values obtained from Equation 2 were employed. The *LS* values were normalized and classified by the Jenks classification method to generate LSM of the study area. A statistical summary of the study area with respect to classified susceptibility levels is given in Table 1. The results were divided into five susceptibility classes as very low, low, moderate, high and very high with Jenks natural breaks algorithm and the final map is presented in Figure 4.

Susceptibility class	Jenks Class	Pixel count of the class	Percentage (%) of the class
Very Low	0 - 0.35	191,896	18.9
Low	0.36 – 0.45	402,378	39.7
Moderate	0.46 – 0.56	244,547	24.1
High	0.56 – 0.7	105,412	10.4
Very High	0.7 – 1.0	69,157	6.8

Table 1. The landslide probability distributions within each class obtained from the FR method.

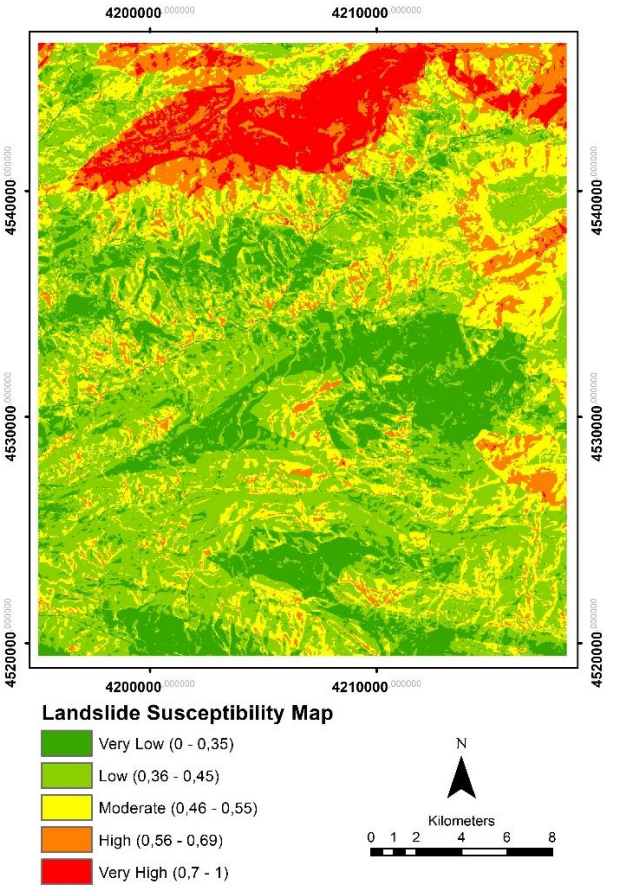

Figure 4. The LSM of the study area.

4. CONCLUSIONS AND FUTURE WORK

Evaluating landslide susceptibility can offer crucial insights to minimize future landslide destruction by aiding informed decisions related to land-use planning, traffic routes, and other hazard and risk assessments. The FR method used here enables the understanding of the relationships between the landslide occurrence and the pre-determined conditioning factors, which form an important basis for the selection of data-driven machine learning methods and optimizing their parameters.

The number of landslides identified from aerial photogrammetric datasets in the study site is over 300. However, their sizes, geological and geomorphological characteristics, and land use land cover properties vary greatly. Altitude, slope, aspect, plan and profile curvature, topographic wetness index, distance to faults, lithology, and land use and land cover have all been identified as significant factors affecting landslide susceptibility. Consideration of these factors is crucial for effective landslide risk assessment, land use planning, and the implementation of appropriate mitigation measures. By incorporating these findings into comprehensive landslide hazard maps and management strategies, we can minimize the adverse impacts of landslides and ensure the safety of communities residing in landslide-prone areas. This study can serve in the selection of data-driven methods used for regressing landslide susceptibility with high accuracy and reliability.

ACKNOWLEDGEMENTS

The first author of this paper was supported by the Higher Education Council of Türkiye (YÖK) within the 100/2000 Programme.

REFERENCES

AFAD (Deprem Ve Risk Azaltma Genel Müdürlüğü Deprem Dairesi Başkanlığı), 2023. 06 Şubat 2023 Pazarcık – Elbistan Kahramanmaraş (Mw: 7.7 – Mw: 7.6) Depremleri Raporu. 140s. https://deprem.afad.gov.tr/assets/pdf/Kahramanmara%C5%9F%20Depremi%20%20Raporu_02.06.2023.pdf

Akbaş, B., Akdeniz, N., Aksay, A., Altun, İ., Balcı, V. et al., 2016. Turkey geological map mineral research & exploration general directorate publication, Ankara, Turkey.

Çıplak, R., 2004. Properties of the East Anatolian Fault Between Erkenek and Gölbaşı (Adıyaman) Area. İstanbul Technical University, MSc thesis, p. 76.

Dao, D. V., Jaafari, A., Bayat, M., Mafi-Gholami, D., Qi, C., Moayedi, H., Phong, T. V., Ly, H.-B., Le, T.-T., Trinh, P. T., Luu, C., Quoc, N. K., Thanh, B. N., & Pham, B. T., 2020. A spatially explicit deep learning neural network model for the prediction of landslide susceptibility. Catena, 188.

EEA. EU-DEM v1.1. https://land.copernicus.eu/imagery-in-situ/eu-dem/eu-dem-v1.1/view (last accessed on 11.04.2023).

HGM. HGM Küre. https://kure.harita.gov.tr/, (last accessed on 11.04.2023).

Karakas, G., Kocaman, S., & Gokceoglu, C., 2021. Aerial Photogrammetry and Machine Learning Based Regional Landslide Susceptibility Assessment for an Earthquake Prone Area in Turkey. The International Archives of the Photogrammetry, Remote Sensing and Spatial Information Sciences, XLIII-B3-2021, 713-720. https://doi.org/10.5194/isprs-archives-XLIII-B3-2021-713-2021

Karakas, G., Kocaman, S., Gokceoglu, C., 2022. On the Effect of DEM Quality for Landslide Susceptibility Mapping. ISPRS Ann. Photogramm. Remote Sens. Spatial Inf. Sci., V-3-2022, 525–531, https://doi.org/10.5194/isprs-annals-V-3-2022-525-2022, 2022.

Khan, H., Shafique, M., Khan, M. A., Bacha, M. A., Shah, S. U., & Calligaris, C., 2019. Landslide susceptibility assessment using Frequency Ratio, a case study of northern Pakistan. The Egyptian Journal of Remote Sensing and Space Science, 22(1), 11-24. https://doi.org/10.1016/j.ejrs.2018.03.004

Nefeslioglu, H. A., Gokceoglu, C., & Sonmez, H., 2012. An assessment on the use of logistic regression and artificial neural networks with different sampling strategies for the preparation of landslide susceptibility maps. Engineering Geology, 128, 62-75.

Pham, B. T., Van Dao, D., Acharya, T. D., Van Phong, T., Costache, R., Van Le, H., Nguyen, H. B. T., & Prakash, I., 2021. Performance assessment of artificial neural network using chi-square and backward elimination feature selection methods for landslide susceptibility analysis. Environmental Earth Sciences, 80(20). https://doi.org/10.1007/s12665-021-09998-5

Reilinger, R., McClusky, S., Vernant, P., Lawrence, S., Ergintav, S., Cakmak, R., Ozener, H., Kadirov, F., Guliev, I., Stepanyan, R., Nadariya, M., Hahubia, G., Mahmoud, S., Sakr, K., ArRajehi, A., Paradissis, D., Al-Aydrus, A., Prilepin, M., Guseva, T., Evren, E., Dmitrotsa, A., Filikov, S.V., Gomez, F., Al-Ghazzi, R. and Karam, G., 2006. GPS constraints on continental deformation in the Africa-Arabia-Eurasia continental collision zone and implications for the dynamics of plate interactions. Journal of Geophysical Research, 111, B05411, doi:10.1029/2005JB004051.

Şaroğlu, F., Emre, Ö. ve Kuşçu, İ. 1992. Active Fault Map of Türkiye, MTA Publications, Ankara.

Sonker, I., Tripathi, J. N., & Swarnim, 2022. Remote sensing and GIS-based landslide susceptibility mapping using frequency ratio method in Sikkim Himalaya. Quaternary Science Advances, 8. https://doi.org/10.1016/j.qsa.2022.100067

Zanaga, D., Van De Kerchove, Ruben, Daems, Dirk, De Keersmaecker, Wanda, Brockmann, Carsten, Kirches, Grit, Wevers, Jan, Cartus, Oliver, Santoro, Maurizio, Fritz, Steffen, Lesiv, Myroslava, Herold, Martin, Tsendbazar, Nandin-Erdene, Xu, Panpan, Ramoino, Fabrizio, & Arino, Olivier, 2022. ESA WorldCover 10 m 2021 v200. https://doi.org/https://doi.org/10.5281/zenodo.7254221

APPENDIX

Factors	Class	N_{Ci}:	N_{Ci}:/ N_{Ct}: (%)	N_{Li}:	N_{Li}:/ N_{Lt}: (%)	FR
Altitude	602.67-791.29	50878	5.02	828	2.41	0.48
	791.29-979.9	229747	22.67	2,470	7.18	0.32
	979.9-1168.52	311018	30.69	3,675	10.68	0.35
	1168.52-1357.14	177965	17.56	4,061	11.80	0.67
	1357.14-1545.76	106193	10.48	11,293	32.81	3.13
	1545.76-1734.38	65680	6.48	6,741	19.59	3.02
	1734.38-1923	37733	3.72	3,188	9.26	2.49
	1923-2111.66	22307	2.20	1,901	5.52	2.51
	2111.66-2300.24	11869	1.17	259	0.75	0.64

Table A1. The FR statistics of the study area for altitude.

Factors	Class	N_{Ci}:	N_{Ci}:/ N_{Ct}: (%)	N_{Li}:	N_{Li}:/ N_{Lt}: (%)	FR
Slope	0-8	292,813	28.89	7,966	23.15	0.80
	8-14	329,216	32.49	7,911	22.99	0.71
	14-20	226,853	22.39	6,517	18.94	0.85
	20-26	114,874	11.34	5,750	16.71	1.47
	26-31	36,702	3.62	3,551	10.32	2.85
	31-37	11,167	1.10	2,089	6.07	5.51
	37-44	1,575	0.16	540	1.57	10.10
	44-60	191	0.02	92	0.27	14.33
Aspect	N	118,969	11.74	1,474	4.28	0.36
	NE	80,425	7.94	1,433	4.16	0.52
	E	80,019	7.90	3,122	9.07	1.15
	SE	128,447	12.67	13,885	40.34	3.18
	S	207,153	20.44	9,047	26.29	1.29
	SW	163,261	16.11	2,315	6.73	0.42
	W	105,749	10.44	1,422	4.13	0.40
	NW	129,367	12.77	1,718	4.99	0.39
Plan Curvature	-6.67--5.56	1	0.00	0	0.00	0.00
	-5.56--4.54	4	0.00	0	0.00	0.00
	-4.54--3.63	3	0.00	0	0.00	0.00
	-3.63--2.59	30	0.00	0	0.00	0.00
	-2.59--1.59	104	0.01	6	0.02	1.70
	-1.59--0.58	1,398	0.14	85	0.25	1.79
	-0.58-0.43	1,006,858	99.36	34,189	99.34	1.00
	0.43-1.5	4,966	0.49	135	0.39	0.80
	1.5-2.46	26	0.00	1	0.00	1.13
Profile Curvature	-3.3--2.35	37	0.00	0	0.00	0.00
	-2.35--1.39	153	0.02	11	0.03	2.12
	-1.39--0.44	6715	0.66	309	0.90	1.35
	-0.44-0.51	1,000,903	98.77	33,894	98.48	1.00
	0.51-1.47	5,180	0.51	175	0.51	0.99
	1.47-2.42	322	0.03	21	0.06	1.92
	2.42-3.38	60	0.01	5	0.01	2.45
	3.38-4.46	15	0.00	1	0.00	1.96
	4.46-5.28	5	0.00	0	0.00	0.00
Topographic Wetness Index	3.27-5.52	40,639	4.01	1290	3.75	0.93
	5.52-7.77	640,038	63.16	17,988	52.27	0.83
	7.77-10.02	24,3515	24.03	10,771	31.30	1.30
	10.02-12.27	61,816	6.10	3,548	10.31	1.69
	12.27-14.53	17,223	1.70	662	1.92	1.13
	14.53-16.78	5,714	0.56	93	0.27	0.48
	16.78-19.03	2,550	0.25	42	0.12	0.48
	19.03-21.3	1,307	0.13	12	0.03	0.27
	21.3-23.53	588	0.06	10	0.03	0.50

Table A2. FR statistics of the study area for slope, aspect, plan curvature, profile curvature, and topographic wetness index.

Factors	Class	N_{Ci}:	N_{Ci}:/ N_{Ct}: (%)	N_{Li}:	N_{Li}:/ N_{Lt}: (%)	FR
Distance to Faults	0-416.08	400,544	39.53	16,770	48.73	1.23
	416.08-831.04	243,165	24.00	11,729	34.08	1.42
	831.04-1248.25	138,105	13.63	4,205	12.22	0.90
	1248.25-1661.7	95,265	9.40	1,236	3.59	0.38
	1661.7-2076.36	60,934	6.01	326	0.95	0.16
	2076.36-2491.11	38,606	3.81	8	0.02	0.01
	2491.11-2906.24	20,775	2.05	48	0.14	0.07
	2906.24-3321.33	12,464	1.23	79	0.23	0.19
	3321.33-3736.48	3,532	0.35	15	0.04	0.13
Lithology	Q (a): Undifferentiated	9,992	0.99	0	0.00	0.00
	Q (b): Alluival fan, debris, moraine	6,320	0.62	8	0.02	0.04
	m1 (a): Clastics and carbonates	25,292	2.50	13	0.04	0.02
	m1 (b): Neritic limestone	3,193	0.32	428	1.24	3.95
	e (a): Neritic Limestone	13,7657	13.58	2,035	5.91	0.44
	k2pn (b): Carbonates and clastics	38,172	3.77	1,065	3.09	0.82
	k2s (b): Pelagic limestone	37,868	3.74	0	0.00	0.00
	k2s (c): Clastics and carbonates (flysch)	28,893	2.85	15	0.04	0.02
	k (a): Neritic limestone	15,848	1.56	21	0.06	0.04
	k (d): Pelagic limestone, clastics, radiolarite, chert etc.	24,931	2.46	0	0.00	0.00
	t2k: Pelagic limestone,radyolarite,chert, clatics etc.	193,147	19.06	1,592	4.63	0.24
	mr: Marble, schist in places	112,399	11.09	21,964	63.82	5.75
	sk: Schist, Calcschist	3,843	0.38	0	0.00	0.00
	of: Undifferentiated basic and ultrabsic rocks	220,5902	22.29	4,799	13.94	0.63
	e2m1: Clastics and carbonates	13,689	1.35	511	1.48	1.10
	e3ol1: Volcanites and sedimentary rocks	80,641	7.96	1,230	3.57	0.45
	e1: Terrigenous clastics	6,507	0.64	78	0.23	0.35
	plQ: Non graded terrigenous clastics	20,462	2.02	98	0.28	0.14
	e1-2: Carbonates and clastics	12,000	1.18	42	0.12	0.10
	e3O: Clastics	4,850	0.48	113	0.33	0.69
	Pe: Clastics	10,051	0.99	404	1.17	1.18
	m3b: Basalt	1,733	0.17	0	0.00	0.00
LULC	Tree cover	151,147	14.91	1,990	5.78	0.39
	Shrubland	7,332	0.72	59	0.17	0.24
	Grassland	637,657	62.92	21,666	62.95	1.00
	Cropland	40,595	4.01	992	2.88	0.72
	Built-up	6,339	0.63	2	0.01	0.01
	Bare / sparse vegetation	168,488	16.63	9,665	28.08	1.69
	Permanent water bodies	1,832	0.18	42	0.12	0.68

Table A3. FR statistics of the study area for distance to faults, lithology, and LULC.